ARMA 10-403

SAND2010-1073C

Application of the Multi-Mechanism Deformation Model for Three-Dimensional Simulations of Salt Behavior for the Strategic Petroleum Reserve

Sobolik, S. R., Bean, J. E., and Ehgartner, B. L.

Sandia National Laboratories, Albuquerque, New Mexico

This paper was prepared for presentation at the 44th US Rock Mechanics Symposium and 5th U.S.-Canada Rock Mechanics Symposium, held in Salt Lake City, UT June 27–30, 2010.

ABSTRACT: The U.S. Strategic Petroleum Reserve stores crude oil in 62 solution-mined caverns in salt domes located in Texas and Louisiana. Historically, three-dimensional geomechanical simulations of the behavior of the caverns have been performed using a power law creep model. Using this method, and calibrating the creep coefficient to field data such as cavern closure and surface subsidence, has produced varying degrees of agreement with observed phenomena. However, as new salt dome locations are considered for oil storage facilities, pre-construction geomechanical analyses are required that need site-specific parameters developed from laboratory data obtained from core samples. The multi-mechanism deformation (M-D) model is a rigorous mathematical description of both transient and steady-state creep phenomena. Recent enhancements to the numerical integration algorithm within the model have created a more stable implementation of the M-D model. This report presents computational analyses to compare the results of predictions of the geomechanical behavior at the West Hackberry SPR site using both models. The recently-published results using the power law creep model produced excellent agreement with an extensive set of field data. The M-D model results show similar agreement using parameters developed directly from laboratory data. It is also used to predict the behavior for the construction and operation of oil storage caverns at a new site, to identify potential problems before a final cavern layout is designed.

1. INTRODUCTION

The U.S. Strategic Petroleum Reserve (SPR) stores crude oil in 62 caverns located at four different sites in Texas (Bryan Mound and Big Hill) and Louisiana (Bayou Choctaw and West Hackberry). The petroleum is stored in solution-mined caverns in salt dome formations. Historically, three-dimensional geomechanical simulations of the behavior of the caverns at SPR facilities have been performed using a power law creep model, which evaluates the secondary steady-state salt creep mechanism. Because the transient creep mechanism is not represented in this model, the common practice has been to use a reduction factor for the elastic modulus. Using this method, and calibrating the creep coefficient to field data such as cavern closure and surface subsidence, analysis agreement with observed phenomena has ranged from adequate to very good, depending upon the degree of homogeneity at a particular site. However, as new salt dome locations are considered for oil and gas storage facilities, pre-construction geomechanical analyses are required that do not rely upon site-specific calibration of parameters obtained from years of field data. These parameters must be developed from laboratory data obtained from core samples at the site; such data include strains measured over a wide range of confining and deviatoric stresses to evaluate steady-state and transient responses.

The multi-mechanism deformation (M-D) model is a rigorous mathematical description of both transient and steady-state creep phenomena. This constitutive model considers three well recognized fundamental features of a creeping material: a steady state creep rate, a transient strain limit, and both a work-hardening and recovery time rate of change (*i.e.,* curvature). Because of the highly non-linear nature of the curvature of the transient strain response, this model has been difficult to integrate in a fully three-dimensional calculation for a model with hundreds of thousands of elements. Many published papers exist presenting two-dimensional calculations using the M-D model, but three-dimensional, large-scale simulations have been more difficult due to the model's high nonlinearity. Recently, enhancements have been completed to the integration algorithm within the model to create a more stable implementation of the M-D model.

This report presents computational analyses to compare the results of predictions of the geomechanical behavior at the West Hackberry SPR site using both the power

law creep and M-D models. The West Hackberry site was chosen because simulations were recently performed using the power law creep model, and they produced very good agreement with an extensive set of field data. The corresponding results using the M-D model show similar agreement using only parameters that were developed directly from laboratory data. The M-D model is also used to predict behavior for the construction and operation of oil storage caverns at a new site under consideration, using parameters developed from an extensive set of laboratory measurements using salt samples from that site. Such a pre-construction analysis can be used to identify potential problems before a final selection of cavern locations is made.

2. M-D MODEL

2.1. Model Description

The Multimechanism Deformation model (M-D) was originally developed by Munson and Dawson [1, 2, 3] and later extended by Munson et al. [4]. It mathematically represents the primary and secondary creep behavior of salt due to dislocations under relatively low temperatures (compared to the melting temperature) and low to moderate stresses which are typical of mining and storage cavern operations. Three micromechanical mechanisms, determined from deformation mechanism maps [1], are represented in the model: 1) a dislocation climb mechanism active at high temperatures and low stresses, 2) an empirically observed mechanism active at low temperatures and low stresses, and 3) a dislocation slip mechanism active at high stresses. These creep mechanisms are assumed to act such that the total steady state creep rate $\dot{\varepsilon}_s$, can be written as the sum of the individual mechanism strain rates.

$$\dot{\varepsilon}_s = \sum_{i=1}^{3} \dot{\varepsilon}_{s_i} \tag{1}$$

The influence of temperature on the creep strain rate is included through an Arrhenius term. The steady state creep strain rates for the first and second mechanisms are identical in form and are implemented using a power law model while the third mechanism (dislocation slip) is represented using an Eyring type model.

$$\dot{\varepsilon}_{s_1} = A_1 \left(\frac{\sigma_{eq}}{G} \right)^{n_1} e^{\frac{-Q_1}{RT}} \tag{2}$$

$$\dot{\varepsilon}_{s_2} = A_2 \left(\frac{\sigma_{eq}}{G} \right)^{n_2} e^{\frac{-Q_2}{RT}} \tag{3}$$

$$\dot{\varepsilon}_{s_3} = \left(B_1 e^{-Q_1/RT} + B_2 e^{-Q_2/RT} \right) \sinh\left[q \left(\frac{\sigma_{eq} - \sigma_0}{G} \right) \right] H\left(\sigma_{eq} - \sigma_0\right) \tag{4}$$

where:

σ_{eq}	equivalent stress
T	temperature (absolute)
G	shear modulus
A_1, A_2, B_1, B_2	structure factors
Q_1, Q_2	activation energies
R	universal gas constant
q	activation volume
σ_0	stress limit
H	Heaviside function with argument $(\sigma_{eq} - \sigma_0)$

From the definition of the Heaviside function, the third mechanism is only active when the equivalent stress exceeds the specified value of the stress limit, σ_0. The equivalent stress appearing in these equations is taken to be the Tresca stress [4]. The Tresca stress can be written in terms of the maximum and minimum principal stresses, σ_1 and σ_3, respectively ($\sigma_1 \geq \sigma_2 \geq \sigma_3$). Alternatively, the Tresca stress may be written as a function of the Lode angle, ψ, and the second invariant, J_2, of the deviatoric stress tensor **s** (whose components are s_{ij}).

$$\sigma_{eq} = \sigma_1 - \sigma_3 = 2\cos\psi\sqrt{J_2} \tag{5}$$

The Lode angle is dependent on both the second and third invariant, J_3, of the deviatoric stress tensor s_{ij}.

$$\psi = \frac{1}{3}\sin^{-1}\left[\frac{-3\sqrt{3}J_3}{2J_2^{3/2}} \right] \qquad -\frac{\pi}{6} \leq \psi \leq \frac{\pi}{6} \tag{6}$$

$$J_2 = \frac{1}{2} s_{ij} s_{ji} \tag{7}$$

$$J_3 = \frac{1}{3} s_{ij} s_{jk} s_{ki} \tag{8}$$

The kinetic equation used in the M-D model is given by Eq. (9) where F is a function which accounts for transient creep effects and $\dot{\varepsilon}_s$ is the steady state dislocation creep strain rate defined by Eq. (1).

$$\dot{\varepsilon}_{eq} = F \dot{\varepsilon}_s \tag{9}$$

The function F has three branches: a work hardening branch ($F > 1$), an equilibrium branch ($F = 1$), and a recovery branch ($F < 1$).

$$F = \begin{cases} \exp\left[\Delta \left(1 - \dfrac{\zeta}{\varepsilon_t^f} \right)^2 \right] & \zeta < \varepsilon_t^f \quad \text{Transient Branch} \\ 1 & \zeta = \varepsilon_t^f \quad \text{Equilibrium Branch} \\ \exp\left[-\delta \left(1 - \dfrac{\zeta}{\varepsilon_t^f} \right)^2 \right] & \zeta > \varepsilon_t^f \quad \text{Recovery Branch} \end{cases} \tag{10}$$

The choice of the particular branch depends on the transient strain limit, ε_t^f, and the internal variable, ζ. The transient strain limit is defined by Eq. (11) where K_0, c, and m are material parameters, T is the absolute temperature, and G is the shear modulus.

$$\varepsilon_t^f = K_0 e^{cT} \left(\frac{\sigma_{eq}}{G} \right)^m \tag{11}$$

The internal variable, ζ, appearing in the calculation of the function F, is obtained by integration of the evolution equation:

$$\dot{\zeta} = \left(F - 1 \right) \dot{\varepsilon}_s \tag{12}$$

The variables Δ and δ, appearing in Eq. (10), are the work hardening and recovery parameters and are given by Eqs. 13 and 14, respectively. In these equations, α, β, α_γ, and β_γ are material parameters. Typically the recovery parameter, δ, is taken to be constant (i.e., $\delta=\alpha_\gamma$).

$$\Delta = \alpha + \beta \log\left(\frac{\sigma_{eq}}{G} \right) \tag{13}$$

$$\delta = \alpha_\gamma + \beta_\gamma \log\left(\frac{\sigma_{eq}}{G} \right) \tag{14}$$

If only the steady state creep response is of interest then the transient and recovery branches may be effectively turned off by setting $\alpha = 0$, $\beta = 0$, $\alpha_\gamma = 0$, $\beta_\gamma = 0$. The M-D model can be further simplified to that of a power law creep model by setting the appropriate structure factors and activation energies to zero. When the M-D model is simplified to only Eq. (3) (the secondary creep mechanism), it becomes the power law creep model that has been used for modeling salt behavior in many applications.

For three dimensional states of stress the components of the creep strain rate tensor are generalized [5] as:

$$\dot{\varepsilon}_{ij}^c = \dot{\varepsilon}_{eq} \frac{\partial \sigma_{eq}}{\partial \sigma_{ij}} \tag{15}$$

Using the Tresca stress in Eq. (5) as the equivalent stress in this form means the creep strains are purely deviatoric ($\dot{\varepsilon}_{ij}^c = \dot{e}_{ij}^c$ since $\dot{\varepsilon}_{kk}^c = 0$) and that all volume change is elastic as defined though the bulk modulus, K (i.e. $\varepsilon_{kk} = \sigma_{kk} / 3K$). Therefore Eq. (15) becomes:

$$\dot{e}_{ij}^c = \dot{\varepsilon}_{eq} \frac{\partial \sigma_{eq}}{\partial \sigma_{ij}} = \dot{\varepsilon}_{eq} N_{ij} \tag{16}$$

Including the bulk and shear moduli, which are both assumed constant, there are a total of 19 parameters used to define the M-D model.

2.2. Numerical Integration of the M-D Model

Traditionally the creep models included in the material libraries of the quasi-static finite element codes at Sandia National Laboratories have used forward Euler integration. Sub-stepping is often needed when the global time step, chosen based on accuracy conditions, is larger than the time step required for stability. Frequently it is necessary to start a simulation with a small time step in order to accurately represent the primary creep behavior. An added benefit of using a small step size is that it often reduces the number of iterations that the nonlinear conjugate gradient solver needs to satisfy for equilibrium of the system.

Once the transient creep phase has passed then it often becomes more efficient to use integration algorithms which are unconditionally stable. The approach used in this work is that whenever the global time step is smaller than the time step required for stability [6, 7] the forward Euler method is used, otherwise the backward Euler method is used. When the backward Euler method is used a system of nonlinear equations must be solved and for this, the Newton-Raphson method is the method of choice.

We assume that the deviatoric stress components, s_{ij}^t, and evolution variable, ζ^t, at time t are known. The goal is to obtain $s_{ij}^{t+\Delta t}$ and $\zeta^{t+\Delta t}$. The generalized trapezoidal rule provides the algorithm for determining $s_{ij}^{t+\Delta t}$ and $\zeta^{t+\Delta t}$. By virtue of the deviatoric nature of the creep strains it is possible to frame the backward Euler problem to one of solving two nonlinear equations for $\sigma_{eq}^{t+\Delta t}$ and $\zeta^{t+\Delta t}$. Once σ_{eq} has been obtained the individual components of the deviatoric stress at the end of the step $s_{ij}^{t+\Delta t}$ or stress tensor $\sigma_{ij}^{t+\Delta t}$ can be obtained.

At this point it is appropriate to highlight some further details of the model implementation. First, to derive the expression for the gradient components, N_{ij}, using the tensor t_{ij}:

$$t_{ij} = s_{ik} s_{kj} - \frac{2}{3} J_2 \delta_{ij} \tag{17}$$

$$N_{ij} = \left(\left[\frac{\cos 2\psi}{\cos 3\psi} \right] \frac{s_{ij}}{\sqrt{J_2}} + \left[\frac{\sqrt{3} \sin \psi}{J_2 \cos 3\psi} \right] t_{ij} \right) \tag{18}$$

Note that Eq. (17) can not be used when $\psi = \pm \pi / 6$ and $\cos(3\psi) = 0$. The conditions $\psi = \pi / 6$ and $\psi = -\pi / 6$ correspond to triaxial compression

$(\sigma_1 = \sigma_2 > \sigma_3)$ and triaxial extension $(\sigma_2 = \sigma_3 < \sigma_1)$ respectively. At these values of Lode angle the gradient is discontinuous, a direct consequence of using the Tresca stress as the equivalent stress. For these values of Lode angle the gradients are computed on each side of $\psi = \pi/6$ or $\psi = -\pi/6$ and then averaged. This is equivalent to replacing the Tresca stress with the von Mises equivalent stress $(\sigma_{eq}^{vm} = \sqrt{3J_2})$ when $\psi = \pm\pi/6$. In this case the gradient is

$$N_{ij} = \frac{3}{2}\frac{s_{ij}}{\sigma_{eq}^{vm}} \quad . \tag{19}$$

When the implicit formulation is used it is necessary to calculate the jacobian elements for use in the Newton-Raphson algorithm. This requires evaluating partial derivatives of N_{ij} with respect to the equivalent stress and internal variable. This poses no particular problem when using Eq. (19) but is especially tedious when $\psi \neq \pm\pi/6$. However, if the Tresca stress and its gradient are expressed in principal stress space then the jacobian elements are easily calculated [8]. The drawback of operating in principal stress space is that the spectral decomposition (principal values and directions) of a 3x3 symmetric matrix needs to be computed. In this application the spectral decomposition is obtained through the use of Jacobi iteration. The Jacobi method has also been used in an implicit implementation of a three-invariant, isotropic-kinematic hardening cap plasticity model [9]. There are other options for performing the spectral decomposition that will likely prove more efficient [e.g. 10] than the current method and they will be examined in the future.

3. WEST HACKBERRY ANALYSES

West Hackberry is located in the extreme southwestern corner of Louisiana, some 15 miles from the Louisiana/Texas border to the west and the Gulf of Mexico to the south. The West Hackberry SPR site began operation in the early 1980s, and comprises five pre-existing caverns (Caverns 6, 7, 8, 9, and 11, known as Phase 1 Caverns, created as early as 1946 for brine storage) and seventeen solution-mined caverns constructed by SPR (numbered 101 through 117, referred to in this paper as Phase 2 caverns). The geological characteristics related to the West Hackberry site are described by a series of reports that illustrate the extent to which geologic site characterization has progressed [11, 12, 13, 14]. The SPR has accumulated many years of measured data at this site pertaining to surface subsidence and cavern closure due to salt creep. These data indicate that the West Hackberry salt dome is a relatively homogeneous salt in terms of its deformation due to creep, thus making it ideal from a modeling perspective for large-scale computational analysis.

A three-dimensional computational analysis of the behavior of the caverns at West Hackberry was recently performed using the power law creep model [15]. The two purposes of this analysis were to calibrate a set of salt creep properties that produce predicted surface subsidence and cavern closure that match measured values, and to use those properties to predict future cavern behavior under a variety of scenarios. This recent analysis developed a set of salt geomechanical properties for the power law creep model that, when used in the geomechanical calculations, produced excellent agreement with the site data. This power law creep analysis was used as the reference point from which the new analysis described in this paper using the M-D model was developed. The following sections include a brief description of the original analysis with the power law creep model, the new analysis with the M-D model, and a comparison of the results from both constitutive models.

3.1. Power Law Creep Analysis

The power law creep analysis is described in greater detail in [15]. For that analysis, a computational domain was developed for the West Hackberry cavern field that encompasses the eastern half of the salt dome, with a vertical symmetry plane through six WH caverns (110, 109, 103, 101, 105, and 117). The mesh for the computational model is illustrated in Figures 1 and 2. Figure 1 shows the entire mesh used for these calculations, and Figure 2 shows the same view with the overburden and caprock removed to expose the salt formation. Four material blocks were used in the model to describe the stratigraphy: the overburden, caprock, salt dome and sandstone surrounding the salt dome. The overburden is made of sand, and the caprock layer is made of gypsum or limestone. Figure 3 shows three views of the layout of the meshed caverns used for these calculations, which includes the six half caverns listed above, plus full cavern representations for 108 and the Phase 1 caverns (6, 7, 8, 9, and 11). The figures show the caverns at their current volumes plus five additional extraction layers, which represent proposed additional salt leaching operations to grow the existing West Hackberry caverns. Five of the caverns on the vertical plane of symmetry (110, 109, 101, 105, and 117) and cavern 108 were constructed in the mesh as frustums with approximate dimensions to the actual caverns. Cavern 103 was created by a mesh-cutting technique to match the cavern geometry developed from sonar measurements. The Phase 1 caverns were created by calculating an average cavern radius as a function of elevation, and developing the profiles into axisymmetric cavern shapes. The coordinates are based on Louisiana field coordinates, and converted to mesh coordinates

with Cavern 103 at the origin, and coordinate axes aligned with compass directions (X-axis for W-E, Y-axis for N-S).

The analysis simulates the excavation of the Phase 1 and Phase 2 caverns, and their subsequent filling with oil according to the historical schedule, for an operational period of 30 years. In general, these caverns have been maintained at constant operating pressures except during workovers. The standard pressure condition applied to each cavern was based on an average wellhead pressure ranging between 6.20 to 6.72 MPa (900 and 975 psi). The simulation also includes a series of five-year cycles of cavern workovers. During the five-year cycle, each cavern is scheduled for a workover, when its wellhead pressure is held at 0 Pa for three months. The pressure for that cavern is returned to its normal operating pressure for the fourth month (so that the workover rig can be moved to a new well) and then the workover of the next scheduled well begins. Previous analyses have shown that operations that create large, abrupt pressure changes in a storage cavern (such as workovers) will induce the greatest potential for dilatant damage in the surrounding salt.

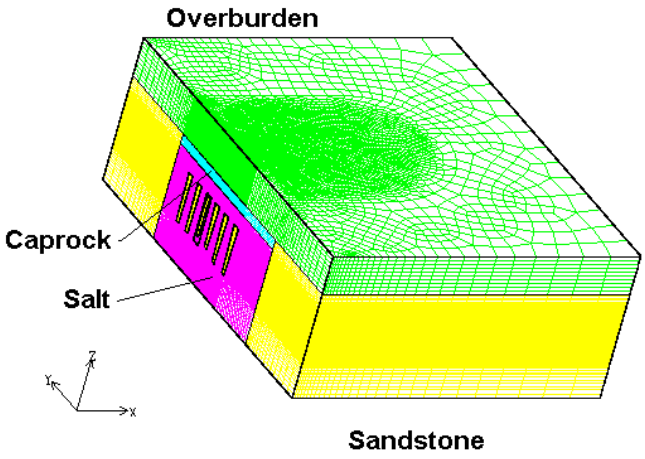

Fig. 1. Computational mesh used for the West Hackberry calculations.

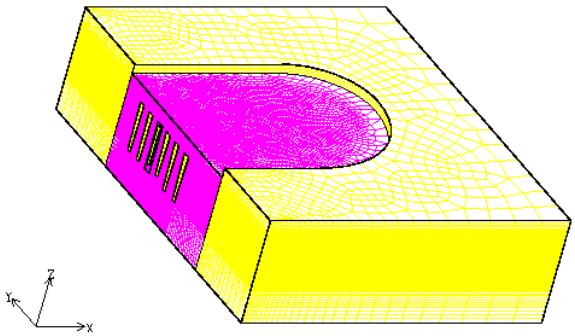

Fig. 2. Computational mesh showing the salt formation and surrounding sandstone.

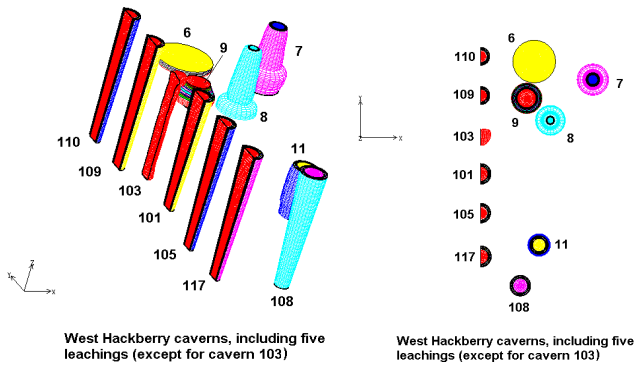

Fig. 3. West Hackberry caverns included in the computational mesh (2 views).

This analysis utilized JAS3D, Version 2.0.F [16], a three-dimensional finite element program developed by Sandia National Laboratories, and designed to solve large quasi-static nonlinear mechanics problems. The power law creep model considers only secondary steady-state creep. The creep steady state strain rate is determined from the effective stress in Eq. (3).

The salt creep properties assume a homogeneous material, and are generally obtained from laboratory measurements. Values for the creep coefficient, the stress exponent, and the thermal activation energy constant for the power law creep model have been obtained for hard and soft salts through mechanical property testing of salt cores collected from boreholes at the SPR sites [17, 18]. The West Hackberry salt is identified in [17] with a group of three SPR "soft" salts, for which an averaged set of properties was obtained; the mechanical properties required and originally used for the power law creep model are listed in Table 1.

Table 1. Power Law Creep Mechanical Properties Used for West Hackberry Salt.

Property	West Hackerry properties [17]
Density, kg/m^3	2300
Elastic modulus, GPa	31.0
Shear modulus, GPa	12.4
Poisson's ratio	0.25
Creep Constant A_2, sec^{-1}	1.13×10^{13}
Exponent n	5.0
Q, cal/mol	10000
Thermal constant Q/R, K	5033

Additionally, an elastic modulus reduction factor (RF) was used to simulate the immediate primary creep response that is not captured in the power law creep model. Based on several previous studies [18, 19, 20], a value for RF of 12.5 was applied to the elastic modulus value in Table 1.

With the original power law creep properties listed in Table 1 and the reduced elastic modulus, the numerical

analysis was performed as described, and predicted values for surface subsidence and cavern closure were obtained from the calculations and compared to site data. Measured surface elevation data over each of the West Hackberry caverns have been obtained since January 1983. The data obtained since 1991, when the mean daily wellhead pressures were increased at the West Hackberry site [21], have been converted to surface subsidence distances over the same period. Figure 4 shows a comparison between measured and predicted surface subsidence at locations directly above the specified caverns. The analysis using the original Munson properties significantly underpredicts the subsidence; a similar result was obtained in an earlier analysis [22]. Cavern volume closure information was obtained between 1990 and 1995 for West Hackberry caverns 101-117 for periods between workovers. Figure 5 compares the cavern closure data to that predicted by the analysis. The analytical closures underpredict the data by a factor of approximately 3.

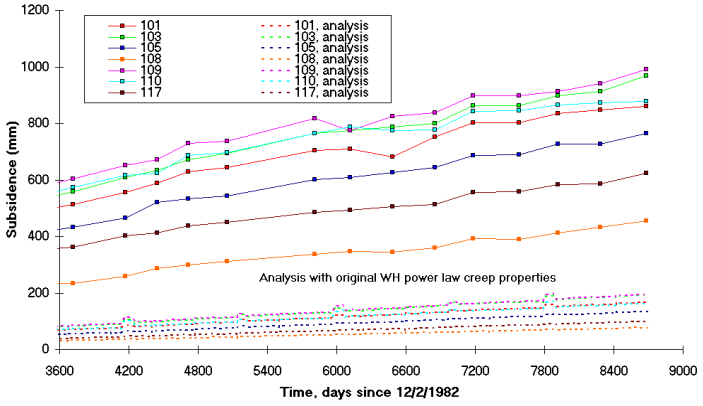

Fig. 4. WH Surface Subsidence Data Compared to Predictions Using WH Salt Properties [17].

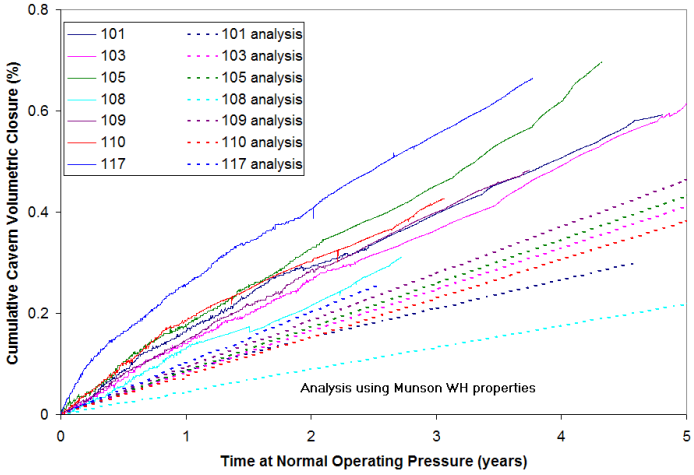

Fig. 5. WH Cavern Volume Closure Data Compared to Predictions Using WH Salt Properties [17].

For the original analysis in [15], one of the requirements was to determine a secondary creep coefficient (A_2) correlated to the surface subsidence and cavern closure data. After several iterations, a value for A_2 equal to 4 times the value given in Table 1 ($4\times A_2 = 4.52\times10^{13}$ sec) was chosen. The numerical analysis was redone with the modified creep coefficient. Figure 6 shows the measured and predicted surface subsidence (similar to Figure 4), using the modified creep coefficient; the new predictions compared very well with the data. Figure 7 compares the measured and predicted cavern volume closure using the modified creep coefficient. The predicted behaviors in Figure 7 are within the range of the data, with predictions for specific caverns ranging from a very good match for Cavern 108 to a 50% overprediction for Cavern 103. There are several explanations for the discrepancies between predicted and measured cavern closure, including the idealized frustum representations of most of the caverns, the heterogeneity of the salt, and the use of a reduced elastic modulus rather than a transient creep mechanism. The modified secondary creep coefficient $4\times A_2$ was selected to be the standard property value for the West Hackberry site when using the power law creep model. [8]

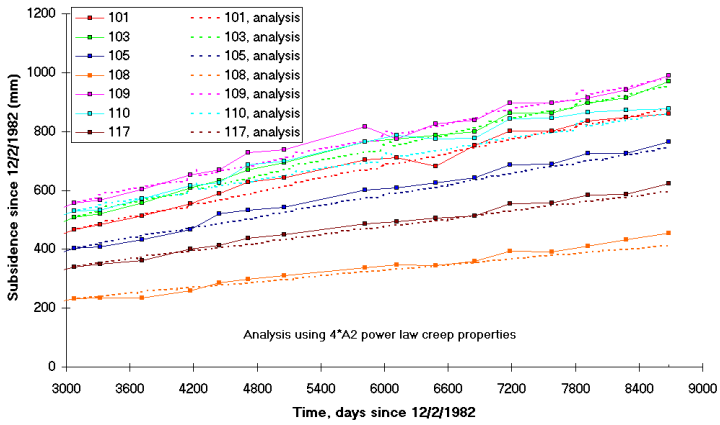

Fig. 6. WH Surface Subsidence Data Compared to Predictions Using Modified Creep Coefficient $4\times A_2$.

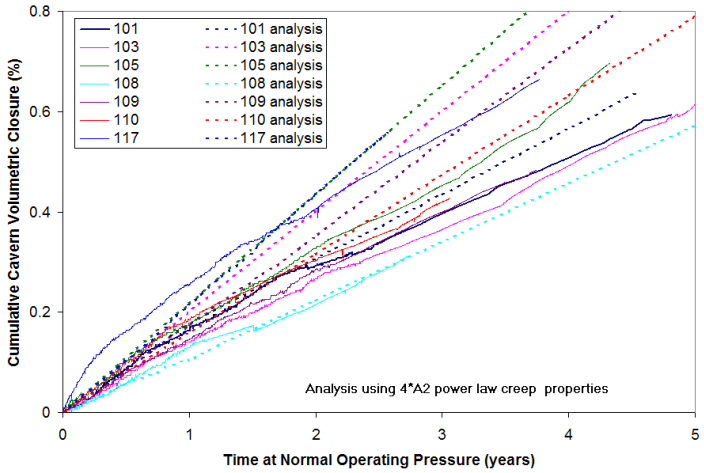

Fig. 7. WH Cavern Closure Data Compared to Predictions Using Modified Creep Coefficient $4\times A_2$.

One of the deficiencies of the power law creep model is illustrated in Figure 8, which shows the predicted cavern closure for a period of 18 years that includes several workovers in each cavern. The workovers are represented by the large increases in closure every five years, due to the decrease in cavern pressure for a three month period. In Figure 8, there is a sharp peak at each increase in closure that is related to the reduced elastic modulus, which is formed when the cavern is repressurized following the workover. The elastic component is small when compared to the creep deformations during the 3 month workover period. Overall it may be unimportant, but when looking at detailed workover behavior, the artificial elasticity before and after the workover period may affect the results. These temporary peaks are even more pronounced in the predictions for the Phase 1 caverns, which comprise much greater diameter-to-height ratios than the more traditionally shaped Phase 2 caverns. Because of this short-term overprediction of cavern closure due to an artificial elastic effect, the power law creep model may be inadequate to model the effects of activities involving large pressure differentials over short time periods on the salt and the well casings. The need to model short-term events in salt caverns provided the impetus to improve the M-D model for use in three-dimensional calculations.

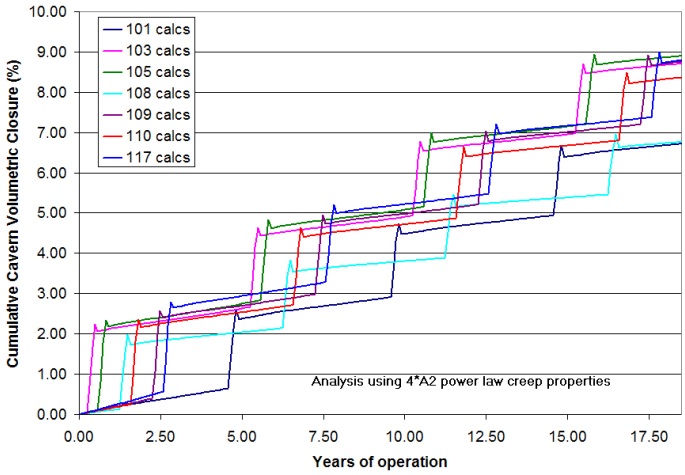

Fig. 8. WH Cavern Closure Predictions Using Modified Creep Coefficient $4\times A_2$.

3.2. M-D Model Analysis

Using the power law creep analysis results as a baseline, the M-D model was then used to attempt to replicate the earlier results using published properties based on laboratory data. The M-D model equations are described by Eqs. (2), (3), (4), (11), (13), and (14). The input properties for these equations are listed in Table 2, and are based on an averaged set of data from three soft salts from SPR storage sites. Although the values specified in [17] were used for the initial M-D calculations, the creep strain rates measured in the laboratory from the West Hackberry core samples were somewhat higher than the average calculated from all the "soft" salt samples. All other aspects of the previous analysis were kept the same.

Table 2. M-D Model Mechanical Properties Used for West Hackberry Salt.

Property	West Hackerry, soft salt properties [17]
Density, kg/m^3	2300
Elastic modulus, GPa	31.0
Shear modulus G, GPa	12.4
Poisson's ratio	0.25
Primary Creep Constant A_1, sec^{-1}	9.81×10^{22}
Exponent n_1	5.5
Q_1, cal/mol	25000
Secondary Creep Constant A_2, sec^{-1}	1.13×10^{13}
Exponent n_2	5.0
Q_2, cal/mol	10000
B_1, sec^{-1}	7.121×10^{6}
B_2, sec^{-1}	3.55×10^{-2}
σ_0, MPa	20.57
q	5335
m	3.0
K_0	6.275×10^{5}
c	0.009198
α	-21.05
β	-7.738
δ	0.58

Figure 9 compares the measured subsidence at the West Hackberry site to the predicted subsidence using the M-D model and the properties in Table 2. The analysis results in a small underprediction of the magnitude of subsidence at each of the monitored locations over a period of fifteen years; these M-D predictions match the site data better than the power law creep predictions using the published value for A_2 (Fig. 4), but not as well as those using the modified coefficient $4\times A_2$ (Fig. 6). Figure 10 compares the measured cavern volume closure to that predicted by the M-D model. A similar result is observed here; the M-D calculations match the site data better than the power law creep model with the unmodified creep coefficient (Fig. 5), but not as well as with the modified creep coefficient (Fig. 7). It can be concluded that the M-D model using the published salt properties in [17] produced a better match to observed field behavior in a "blind" analysis than using the power law creep model with the same published secondary creep parameters and modified modulus. The M-D model may require a similar adjustment of selected properties to match phenomena measured in the field, but it can be used to project long-term behavior in the same way that the power law creep model has been used.

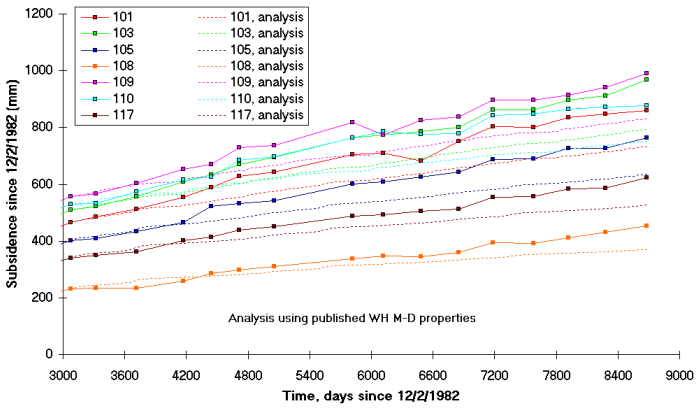

Fig. 9. WH Surface Subsidence Data Compared to Predictions Using WH M-D Salt Properties [17].

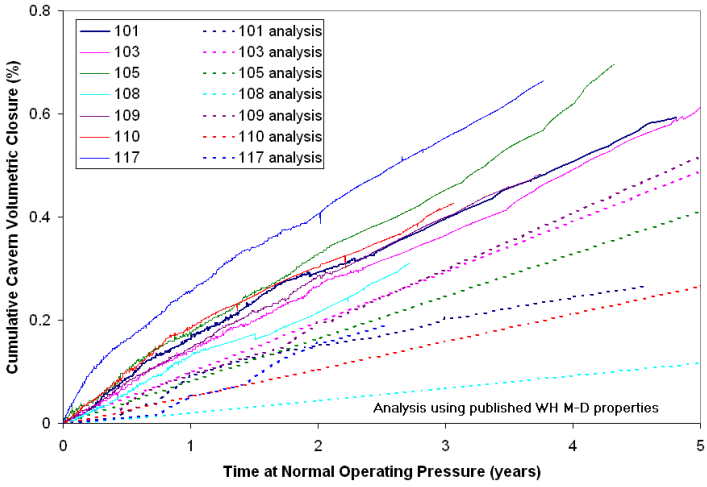

Fig. 10. WH Cavern Volume Closure Data Compared to Predictions Using WH M-D Salt Properties [17].

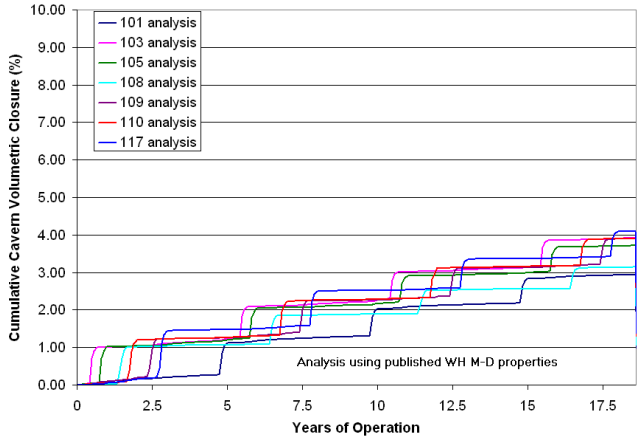

Fig. 11. WH Cavern Closure Predictions Using Published M-D Properties [17].

Figure 11 shows the cavern closure for a period of 18 years predicted using the M-D model that includes several workovers in each cavern (analogous to Fig. 8 with the power law creep model). The artificial peaks observed at the beginning of each workover using the power law creep model are absent in the M-D model calculations, which would indicate a more realistic portrayal of the behavior of the salt around the cavern during periods of large, short-term pressure changes. This feature makes the M-D model attractive for modeling short time period events such as a cavern integrity test, a workover, or a sudden change in stress in the salt due to a fracture.

The salt properties published in [17] for soft salts, including West Hackberry, were averaged from samples obtained from several sites. Munson indicated that the West Hackberry samples exhibited higher creep rates than would be predicted using the averaged values. Therefore, it was decided to determine if a multiplying factor could be applied to the M-D properties much like what was done for the power law creep analyses [15], by applying a factor of 4 to the creep coefficient. Two methods were chosen to try to use the M-D model to match the data. First, a set of calculations was performed using a factor applied to the secondary creep coefficient A_2, as was done in [15]. A multiplier of 1.57 was selected for these calculations. Second, it was decided to evaluate the transient component of the M-D model by applying a multiplier to the transient strain rate coefficient K_0 in Eq. (11). A transient creep multiplier of 1.7 was selected for this second set of calculations. Figs. 12 through 17 plot the same comparisons as did Figs. 9-11: Figs. 12 through 14 are for the case of the M-D model with $1.57 \times A_2$, and Figs. 15 through 17 for the case of the M-D model with $1.7 \times K_0$. The predicted surface subsidence in Figures 12 and 15 match the measured results as well as the power law creep predictions in [15]. For a relatively homogeneous salt, surface subsidence is probably the easiest set of data to predict because of the spatially distributed effect of salt deformation from the caverns to the surface. Figures 13 and 16 show similar improvements in predicted cavern volume closure, although these data are slightly underpredicted by both sets of calculations. The plots of cavern volume closure over 18 years of operations, as shown in Figs. 14 and 17, are very similar to each other. From these two sets of calculations, it is difficult to observe which property modification – multiplying the secondary creep coefficient or the transient creep coefficient – is the preferable method for matching the observed physical behavior. It may be necessary to perform these calculations with more physically representative geometries for the Phase 2 caverns. It is also possible that the spatial variability in salt mechanical properties is more important in predicting cavern closure than in subsidence, and thus some allowance for this variability will need to be included in analyzing cavern behavior in a salt dome.

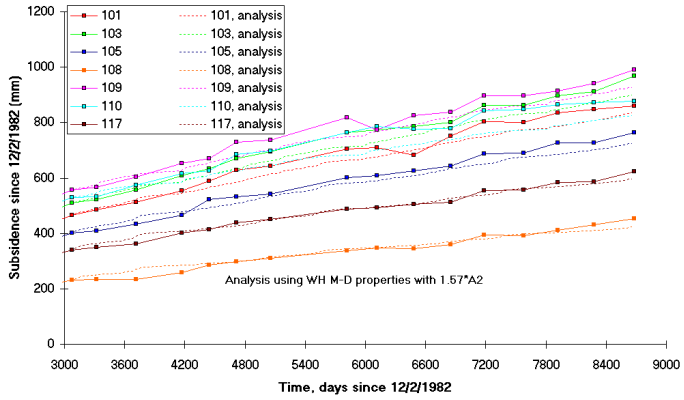

Fig. 12. WH Surface Subsidence Data Compared to Predictions Using M-D Model, $1.57 \times A_2$.

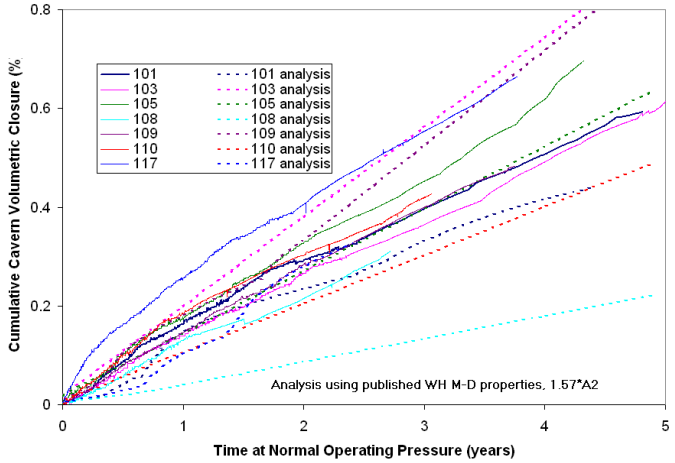

Fig. 13. WH Cavern Volume Closure Data Compared to Predictions Using M-D Model, $1.57 \times A_2$.

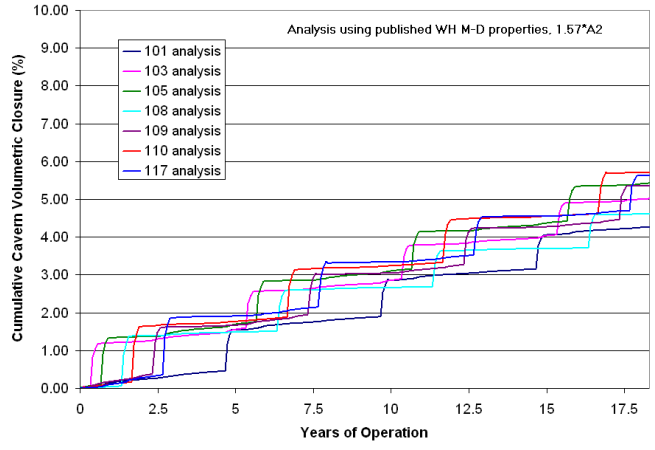

Fig. 14. WH Cavern Closure Predictions Using M-D Properties with $1.57 \times A_2$.

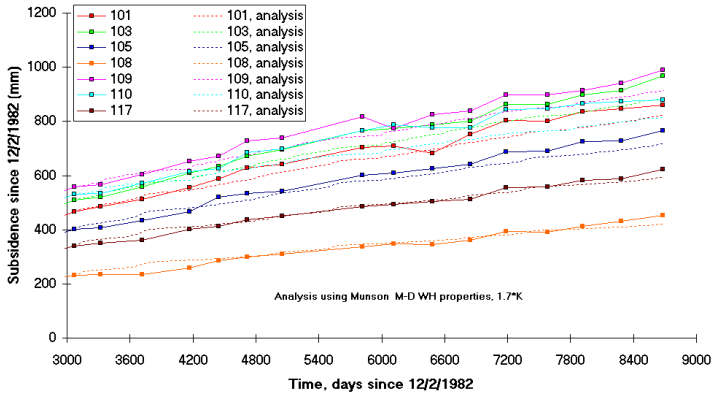

Fig. 15. WH Surface Subsidence Data Compared to Predictions Using M-D Model, $1.7 \times K_0$.

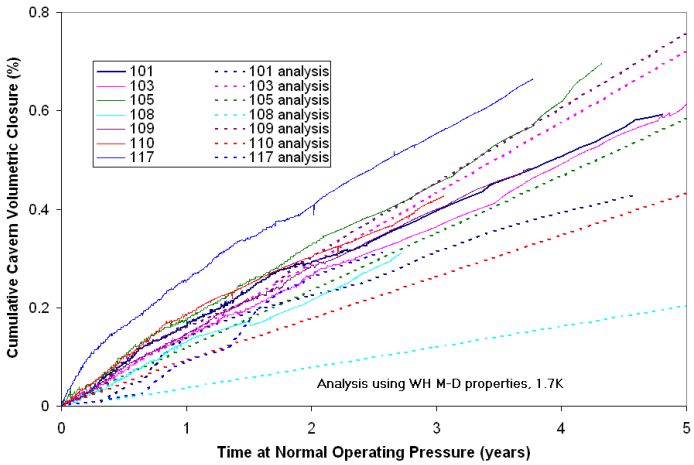

Fig. 16. WH Cavern Volume Closure Data Compared to Predictions Using M-D Model, $1.7 \times K_0$.

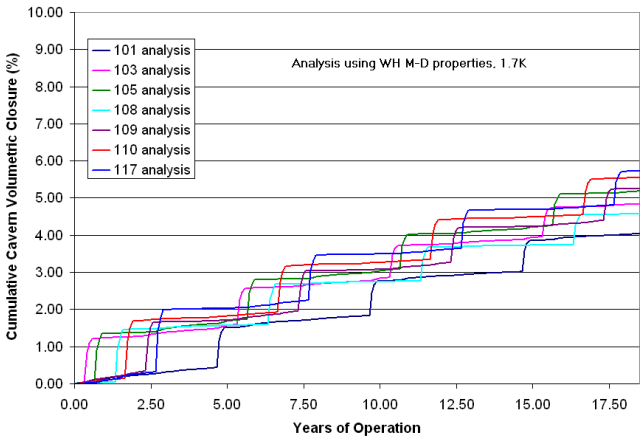

Fig. 17. WH Cavern Closure Predictions Using M-D Properties with $1.7 \times K_0$.

Any model to be used for an analysis of the geomechanical behavior of a salt dome requires mechanical property data obtained from laboratory testing of salt, preferably from samples from that site. Using published properties based on the same laboratory data set, the calculations using the M-D model produced

predictions of geomechanical behavior at West Hackberry that more closely matched field measurements than did the same analysis with the power law creep model. This increased ability to rely on laboratory data to model the mechanical properties of the salt increases the confidence of using the M-D model for pre-construction site characterization or for long-term prediction of behavior at existing storage sites. The two potential drawbacks in using the M-D model are insufficient laboratory data to obtain the full suite of properties, and CPU time; due to its required implementation of smaller time steps, the M-D calculations shown here used approximately four times the CPU time as the power law creep calculations.

4. RICHTON ANALYSIS

In 2005, as the uncertain nature of the United States' oil supply became more apparent due to the continuing conflicts in the Middle East and because of damage to the petroleum industry resulting from hurricanes on the Gulf Coast, Congress passed the Energy Policy Act of 2005. One of the directives of that act was to increase the capacity of the SPR from 700 million barrels (MMB) to 1.0 billion barrels. In June 2007, the U.S. Department of Energy (DOE) issued an SPR Expansion Plan [23] which included the identification of a salt dome near Richton, Mississippi, as a potential SPR expansion site. The DOE began a program to characterize the Richton site to determine its suitability for the construction of a storage facility. One of the aspects of that site characterization was a pre-construction analysis of the in situ stress state in the salt dome and surrounding rock structure. Knowledge of the stress-state in the near-field vicinity of the Richton salt dome, at present, is important to understanding the pre-excavation oil storage conditions so that feasible mining and construction operations can be conducted.

As part of the Richton site characterization study, a set of M-D mechanical properties were derived from several studies of Richton salt from the 1980s [24, 25, 26] and a new set of laboratory data from Richton core samples [27, 28]. These data were used to develop a property set incorporated into geomechanical analyses of the Richton dome for its potential use as a petroleum storage site [29]. The analyses in [29] comprised several scenarios. The computations included four different mesh geometries: a two-dimensional axisymmetric mesh; a three-dimensional mesh with vertical planes of symmetry and either a cylindrical or tapered dome structure; and a three-dimensional mesh based on seismic surveys of the dome. The simulated operational scenarios in [29] included either 19 or 31 caverns in the salt dome. Finally, dilatant damage criteria were used that were based on different qualities of salt found at Richton [27, 28]. The power law creep model with reduced modulus was primarily used in [29], with the exception of a two-dimensional calculation using the M-D model (these results are also described in detail in [30]). After the completion of the original site characterization study, the newly-modified M-D model in JAS3D was completed, and a new set of calculations was performed. The new calculations utilized the same mesh and operational scenario as a simulation in [29] using a three-dimensional mesh with vertical planes of symmetry. The mesh for the computational model is illustrated in Figure 18. The 30-degree wedge format with five caverns, a cylindrical salt dome and upper flange, and vertical planes of symmetry was designed to simulate a storage facility with 31 caverns. Figure 18 refers to Caverns 1, 2, 3, 4, and 5; Cavern 1 represents one cavern, at the center of the 31-cavern field, Caverns 2, 3, and 4 each represent 6 caverns in the field due to model symmetry, and Cavern 5 represents a ring of 12 caverns due to the same symmetry.

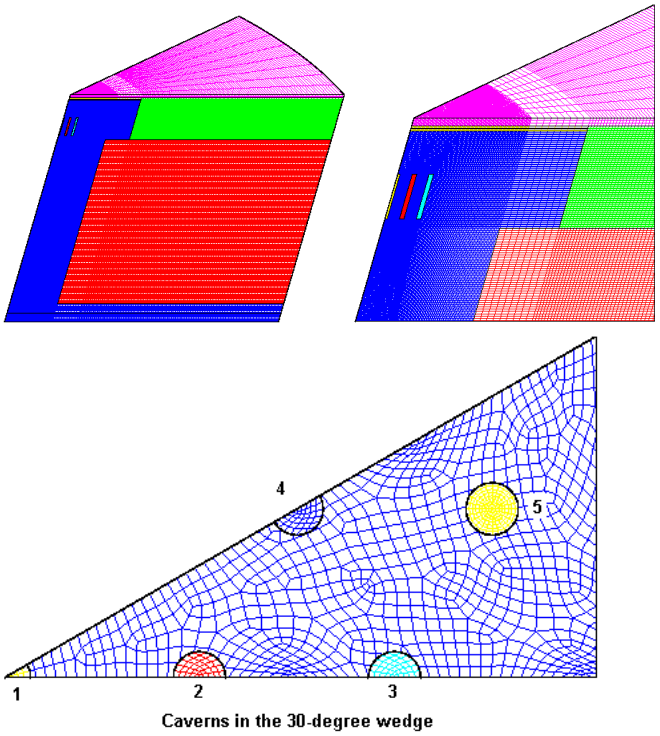

Fig. 18. Three-dimensional finite element mesh for 30-degree wedge, cylindrical salt dome structure with cylindrical flange, for the Richton simulations.

Figure 19 compares the predicted surface subsidence in the middle of the cavern field using the two models. The M-D model predicts significantly greater surface subsidence than the power law creep model, which is probably in part the result of the shallow depth of the top of the Richton dome. Figures 20 and 21 compare the predicted cavern volume closure for the two simulations. The predictions are nearly equal for the two models, with the M-D model lacking the artificial peaks in closure predicted by the power law creep model. In this

model, the subsided volume should roughly equal the closure volume of the caverns. In order to conserve volume, the shape of the subsidence troughs differ between the analyses, with the MD model producing larger subsidence magnitudes focused in the central portion of the field. Predicting the true shape of the subsidence trough is important to estimating the strains imposed on surface infrastructure. Finally, a prediction of the occurrence of maximum potential for dilatant damage in the salt (as measured by the minimum dilatant damage factor in the salt as a function of time) is shown in Figure 22. The dilatant damage factor is the ratio between J2 and I1 when compared to a damage curve based on laboratory data; in this case, the curve was derived from Richton samples [27]. A value <1 indicates the onset of dilatant damage, and a safety factor of 1.5 is usually considered reasonable. The localized minima occur during workovers at one of the five caverns. Note that there is not a substantial difference in the minimum values achieved by the two models. The results from the M-D model lead to essentially the same conclusions as the power law creep results [29], with the exception of a greater concern about potential well strains due to the larger subsidence values.

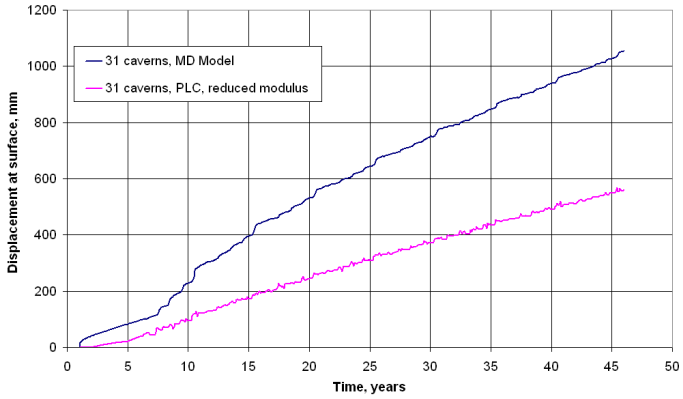

Fig. 19. Predicted surface subsidence over Cavern 1 for the Richton simulations.

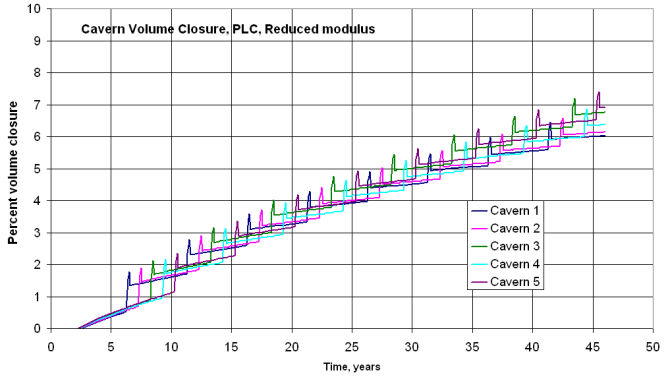

Fig. 20. Predicted cavern volume closure using the power law creep model for the Richton simulations.

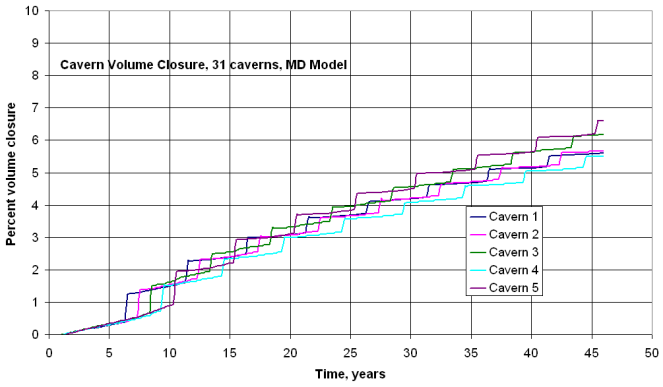

Fig. 21. Predicted cavern volume closure using the M-D model for the Richton simulations.

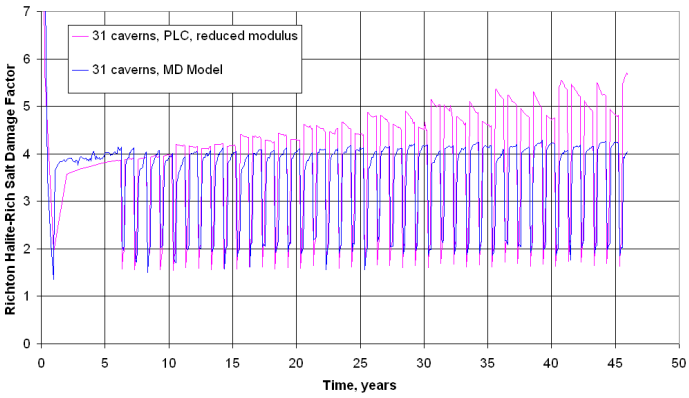

Fig. 22. Predicted minimum dilatant damage factor in salt for the Richton simulations.

5. CONCLUSIONS

The M-D model for evaluating salt creep has existed for many years, but only in recent years has its capabilities been usable in large three-dimensional, parallelized computational models. The recent improvements to the integration algorithm within the model, described in this paper, now allow the full effect of this model to be available for both site characterization studies and simulations involving short-term, large pressure-change events. The new implementation of this model has been tested with previous calculations and found to produce satisfactory predictions of long time period phenomena such as subsidence and volume closure, while also improving the physical representation of short–term events. The M-D model can now be used when sufficient laboratory data are available to develop the required suite of mechanical properties.

Sandia is a multiprogram laboratory operated by Sandia Corporation, a Lockheed Martin Company, for the United States Department of Energy's National Nuclear Security Administration under Contract DE-AC04-94AL85000.

REFERENCES

1. Munson, D.E. and P.R. Dawson, 1979. *Constitutive Model for the Low Temperature Creep of Salt (With Application to WIPP).* SAND79-1853, Sandia National Laboratories, Albuquerque, New Mexico.
2. Munson, D.E. and P.R. Dawson. 1982. *A Transient Creep Model for Salt during Stress Loading and Unloading.* SAND82-0962, Sandia National Laboratories, Albuquerque, New Mexico.
3. Munson, D.E. and P.R. Dawson, 1984. Salt Constitutive Modeling using Mechanism Maps. *1st International Conference on the Mechanical Behavior of Salt, Trans Tech Publications*, 717-737, Clausthal, Germany.
4. Munson, D.E., A.F. Fossum, and P.E. Senseny. 1989. *Advances in Resolution of Discrepancies between Predicted and Measured in Situ WIPP Room Closures*. SAND88-2948, Sandia National Laboratories, Albuquerque, New Mexico.
5. Fossum, A.F., G.D. Callahan, L.L. Van Sambeek, and P.E. Senseny. 1988. How Should One-Dimensional Laboratory Equations be Cast in Three-Dimensional Form? *Key Questions in Rock Mechanics: Proceedings of the 29th U.S. Symposium.* Brookfield, MA: McGraw-Hill Book Company.
6. Zienkiewcz, O.C. and I.C. Cormeau. 1974. Visco-plasticity, Plasticity and Creep in Elastic Solids: A Unified Numerical Solution Approach. *International Journal for Numerical Methods in Engineering*. 8: 821-845.
7. Cormeau, I.C. 1975. Numerical Stability in Quasi-Static Elasto/Visco-Plasticity. *International Journal for Numerical Methods in Engineering*, 9: 109-127.
8. Borja, R.I., K.M. Sama, and P.F. Sanz. 2003. On the Numerical Integration of Three-Invariant Elastoplastic Constitutive Models. *Computer Methods in Applied Mechanics and Engineering*, 192: 1227-1258.
9. Foster, C.D., R.A. Regueiro, A.F. Fossum, and R.I. Borja. 2005. Implicit Numerical Integration of a Three-Invariant Isotropic/Kinematic Hardening Cap Plasticity Model for Geomaterials. *Computer Methods in Applied Mechanics and Engineering*, 194: 5109-5138.
10. Scherzinger, W.M. and C.R. Dohrmann. 2008. A Robust Algorithm for Finding the Eigenvalues and Eigenvectors of 3x3 Symmetric Matrices. *Computer Methods in Applied Mechanics and Engineering*, 197: 4007-4015.
11. Whiting, G. H. 1980. *Strategic Petroleum Reserve (SPR): Geological Site Characterization Report, West Hackberry Salt Dome.* SAND80-7131, Sandia National Laboratories Albuquerque, New Mexico.
12. Magorian, T.R., J.T. Neal, S. Perkins, Q.J. Xiao, and K.O. Byrne. 1991. *Strategic Petroleum Reserve Additional Geologic Characterization Studies West Hackberry Salt Dome, Louisiana.* SAND90-0224, Sandia National Laboratories, Albuquerque, New Mexico.
13. Rautman, C.A., J.S. Stein, and A.C. Snider. 2004. *Conversion of the West Hackberry Geological Site Characterization Report to a Three-Dimensional Model*. SAND2004-3981, Sandia National Laboratories, Albuquerque, New Mexico.
14. Rautman, C.A. and A.C. Snider. 2007. *Sonar Atlas of Caverns Comprising the U.S. Strategic Petroleum Reserve Volume 4: West Hackberry Site, Louisiana*. SAND2007-6051, Sandia National Laboratories, Albuquerque, New Mexico.
15. Sobolik, S.R. and B.L. Ehgartner. 2009. *Analysis of Cavern Stability at the West Hackberry SPR Site*. SAND2009-2194, Sandia National Laboratories, Albuquerque, New Mexico.
16. Blanford, M.L., M.W. Heinstein, and S.W. Key, 2001. *JAS3D. A Multi-Strategy Iterative Code for Solid Mechanics Analysis. User's Instructions, Release 2.0*. SEACAS Library, JAS3D Manuals, Computational Solid Mechanics / Structural Dynamics, Sandia National Laboratories, Albuquerque, New Mexico.
17. Munson, D.E. 1998. *Analysis of Multistage and Other Creep Data for Domal Salts*. SAND98-2276, Sandia National Laboratories, Albuquerque, New Mexico.
18. Munson, D.E. 1999. *Multimechanism-Deformation Parameters of Domal Salts Using Transient Creep Analysis*. SAND99-2104, Sandia National Laboratories, Albuquerque, New Mexico.
19. Morgan, H.S. and R.D. Krieg, 1990. *Investigation of an Empirical Creep Law for Rock Salt that Uses Reduced Elastic Moduli*, SAND89-2322C, presented at the 31st U.S. Symposium on Rock Mechanics held in the Colorado School of Mines in June 18-20, 1990, Sandia National Laboratories, Albuquerque, New Mexico.
20. Wawersik, W.R. and D.H. Zeuch, 1984. *Creep and Creep Modeling of Three Domal Salts – A Comprehensive Update*. SAND84-0568, Sandia National Laboratories, Albuquerque, New Mexico.
21. Woodrum, S., 2001. Cavern Integrity Report Pressure Data---Graphed. Letter Report to B.L. Ehgartner dated April 23, 2001.
22. Ehgartner, B.L. and S.R. Sobolik, 2002. *3-D Cavern Enlargement Analyses*. SAND2002-0526, Sandia National Laboratories, Albuquerque, New Mexico.
23. DOE (United States Department of Energy), 2007. "Strategic Petroleum Reserve Plan – Expansion to One Billion Barrels," Submitted to Congress Pursuant to the Energy and Conservation Act, as Amended., June 2007. Washington, D.C.**:** United States Department of Energy, Office of Petroleum Reserves.
24. Haag, R.D., and Swanson, O.E.. 1983. "Characterization of Earth Materials properties for Conceptual Design of an Exploratory Shaft, Richton Dome, Mississippi," In *Scientific Basis for Nuclear Waste*

management VII. Proceedings of the Seventh Internal Symposium, 14-17, Boston, Massachusetts.

25. Pfeifle, T.W., Mellegard, K.D., and Senseny, P.E., 1983a. *Preliminary Constitutive Properties for Salt and Nonsalt Rock from Four Potential Repository Sites*. ONWI-450, Office of Nuclear Waste Isolation, Columbus, Ohio.

26. Pfeifle, T.W., Mellegard, K.D., and Senseny, P.E., 1983b. *Constitutive Properties of Salt from Four Sites (Technical Report prepared by RE/SPEC Inc.).* ONWI-314, Office of Nuclear Waste Isolation, Columbus, Ohio**.**

27. Broome, S.T., S.J. Bauer, D. Dunn, J.H. Hofer, and D.R. Bronowski, 2009. *Geomechanical Testing of MRIG-9 Core for the Potential SPR Siting at the Richton Salt Dome*. SAND2009-0852, Sandia National Laboratories, Albuquerque, New Mexico.

28. Bauer, S.J., and S.T. Broome, 2010. *Revised Results for Geomechanical Testing of MRIG-9 Core for the Potential SPR Siting at the Richton Salt Dome*. SAND2010-0658, Sandia National Laboratories, Albuquerque, New Mexico.

29. Sobolik, S.R., J.S. Rath, J.G. Arguello, and B.L. Ehgartner, 2009. *Evaluating the In Situ and Operational Stress States for a Potential Strategic Petroleum Reserve Site at Richton, Mississippi*. SAND2009-6137, Sandia National Laboratories, Albuquerque, New Mexico.

30. Rath, J.S., J.G. Argüello, C.M. Stone, and S.R. Sobolik, 2009. *Evaluating the Present in-situ Stress-State for the Richton, MS, Strategic Petroleum Reserve Site using Geomechanical Analyses*, ARMA-09-076, in the *Proceedings for the 43rd US Rock Mechanics Symposium and 4th U.S.-Canada Rock Mechanics Symposium*, Asheville, North Carolina.